2011

Triggering of volcanic activity by large earthquakes

Dulcinea M. Avouris
Michigan Technological University

TRIGGERING OF VOLCANIC ACTIVITY BY LARGE EARTHQUAKES

By

Dulcinea M. Avouris

A THESIS

Submitted in partial fulfillment of the requirements for the degree of

MASTER OF SCIENCE

(Geophysics)

MICHIGAN TECHNOLOGICAL UNIVERSITY

2011

This thesis, "Triggering of Volcanic Activity by Large Earthquakes," is hereby approved in partial fulfillment of the requirements for the Degree of MASTER OF SCIENCE IN GEOPHYSICS.

Department of Geological and Mining Engineering and Sciences

Signatures:

Thesis Co-Advisor:

Dr. Gregory P. Waite

Thesis Co-Advisor:

Dr. Simon A. Carn

Committee Member:

Dr. Michael J. Falkowski

Department Chair:

Dr. Wayne D. Pennington

Date:

Table of Contents

List of Figures

List of Tables

Abstract

Statistical analyses of temporal relationships between large earthquakes and volcanic eruptions suggest seismic waves may trigger eruptions even over great (>1000 km) distances, although the causative mechanism is not well constrained. In this study the relationship between large earthquakes and subtle changes in volcanic activity was investigated in order to gain greater insight into the relationship between dynamic stresses propagated by surface waves and volcanic response. Daily measurements from the Ozone Monitoring Instrument (OMI), onboard the Aura satellite, provide constraints on volcanic sulfur-dioxide (SO_2) emission rates as a measure of subtle changes in activity. Time series of SO_2 emission rates were produced from OMI data for thirteen persistently active volcanoes from 1 October 2004 to 30 September 2010. In order to quantify the affect of earthquakes at teleseismic distances, we modeled surface-wave amplitudes from the source mechanisms of moment magnitude (M_w) ≥7 earthquakes, and calculated the Peak Dynamic Stress (PDS). We assessed the influence of earthquakes on volcanic activity in two ways: 1) by identifying increases in the SO_2 time series data and looking for causative earthquakes and 2) by examining the average emission rate before and after each earthquake. In the first, the SO_2 time series for each volcano was used to calculate a baseline threshold for comparison with post-earthquake emission. Next, we generated a catalog of responses based on sustained SO_2 emission increases above this baseline. Delay times between each SO_2 response and each prior earthquake were analyzed using both the actual earthquake catalog, and a randomly generated catalog of earthquakes. This process was repeated for each volcano. Despite varying multiple parameters, this analysis did not demonstrate a clear relationship between earthquake-generated PDS and SO_2 emission. However, the second analysis, which was based on the occurrence of large earthquakes indicated a response at most volcanoes. Using the PDS calculations as a filtering criterion for the earthquake catalog, the SO_2 mass for each volcano was analyzed in 28-day windows centered on the earthquake origin time. If the average SO_2 mass after the earthquake was greater than an arbitrary percentage of pre-earthquake mass, we identified the volcano as having a response to the event. This window analysis provided insight on what type of volcanic activity is more susceptible to triggering by dynamic stress. The volcanoes with very open systems included in this study, Ambrym, Gaua, Villarrica, Erta Ale and, Turrialba, showed a clear response to dynamic stress while the volcanoes with more closed systems, Merapi, Semeru, Fuego, Pacaya, and Bagana, showed no response.

1. Introduction

Remote triggering of microseismicity by large shallow earthquakes has been documented in a variety of tectonic settings and distances(e.g. Hill et al. 2002). The coseismic offset produced by large events result in a static change in state-of-stress within a few fault lengths of the source. Transient, or dynamic, stress changes which are propagated by seismic waves, can occur up to thousands of kilometers away. While teleseismic triggering of microseismicity has been documented for a number of large (Hill 2008), changes in volcanic systems are difficult to quantify in a robust manner, given the inherent complexities and unpredictable behavior of volcanoes. Despite these difficulties, there is a growing body of research suggesting linked activity on various timescales (e.g. Linde and Sacks 1998; Manga and Brodsky 2006; Cigolini et al. 2007; Harris and Ripepe 2007; Thomas R. Walter and Amelung 2007; Walter et al. 2007; Eggert and Walter 2009; Walter et al. 2009; Watt et al. 2009; De la Cruz-Reyna et al. 2010; Delle Donne et al. 2010). An analysis of the temporal relationship between large earthquakes and volcanic eruptions by Linde and Sacks (1998) showed that eruptions are statistically more likely to happen within 5 days of a large earthquake than any other time. Their analysis was limited to eruptions with a Volcanic Explosivity Index (VEI) ≥2, and earthquakes with M_w ≥7. In a comprehensive review paper on the connection between large earthquakes and volcanic activity, Manga and Brodsky (2006) discussed the effects of both static and dynamic stress as well as possible mechanisms for triggering seismic waves. Several other studies have documented changes in behavior at volcanoes following earthquakes, including increases in thermal flux. A large-scale study by Delle Donne et al. (2010) found an increase in volcanic heat flux in response to regional earthquakes over a 7-year time span (2000-2006). Thirty-seven volcanoes responded to regional (<750 km) earthquakes with an increase in heat flux within 21days of the earthquake. In a study focused on the effect from the M_w 6.4 earthquake in Java on 26 May 2006, Harris et al. (2007) used MODIS data to demonstrate a connection between the earthquake and increased heat flux, at both Merapi (~50 km from the epicenter) and Semeru (~280 km from the epicenter), beginning about three days after the quake. And in late 2002, three separate volcanic systems in Italy (Etna, Stromboli, and Panarea Is.) showed unusual behavior following a series of tectonic earthquakes near Sicily (Walter et al. 2009). This behavior included the first fissure eruption at Mt. Etna since 1947, along with surface fracturing, which had not occurred for decades. Degassing from three distinct areas occurred at Panarea for the first time since 1865, and a dike-fed effusive eruption occurred at Stromboli, the first since 1985. Quantifiable measurements of changes in both the earthquake-generated state-of-stress, and volcanic activity may provide greater insight into the triggering mechanism as well as the types of volcanoes that may be more susceptible to triggering.

In addition to triggering eruptions, large earthquakes can also trigger small earthquakes and tremor at great distances. In the case of the 2002 Denali earthquake, small earthquakes were

triggered in hydrothermal and volcanic areas across the western U.S., and seismic tremor was triggered along the San Andreas fault system in southern California, over 3000 km away. The response to the trigger varies in delay time, duration and amplitude depending on several factors, including surface wave amplitude (Hill et al. 1993; Prejean et al. 2004). While the effect of static stress is strictly limited to near-source distances, decaying at a rate of $1/r^3$, dynamic stresses caused by propagating seismic waves decays at a rate of about $1/r^{1.66}$, making them more likely to be responsible for triggering at large distances (Manga and Brodsky 2006).

Previous studies of earthquake-volcano interaction at teleseismic distances have relied on arbitrary earthquake magnitude and distance cut-offs to characterize the relationship. These studies do not account for the effects of fault geometry and seismic-wave radiation patterns on amplitudes. In this study, we go beyond simply examining the earthquake magnitude and distance from volcano by modeling surface wave propagation from each source to each volcano in the study. Surface wave modeling and the associated Peak Dynamic Stress (PDS) calculations provide a more robust method for identifying which earthquakes may be most influential in triggering a change in activity.

Volcanoes commonly emit gas, even when they are not erupting, through degassing of volatile-rich magma at depth and transport to the surface. The most common components of volcanic gas are typically water vapor (H_2O), carbon dioxide (CO_2), and sulfur dioxide (SO_2). Water and CO_2 are also ubiquitous components of the atmosphere, and therefore challenging to measure in volcanic plumes. However, atmospheric background levels of SO_2 are very low (away from major sources of anthropogenic pollution such as coal-fired power plants and smelters). This makes it an excellent indicator of volcanic degassing because it is easily distinguishable. Both ground-based and satellite measurements of SO_2 have been used to assess volcanic activity on varying time scales (Fischer et al. 2002; Carn et al. 2008). In this study we use daily estimates of volcanic SO_2 emissions from the Ozone Monitoring Instrument (OMI) on NASA's Aura satellite. Ground-based measurements with temporal resolution are impossible at most volcanoes. These emission rates provide a consistent proxy for volcanic activity that we can compare with PDS estimates.

2. Methodology

The investigation required quantitative measures of both volcanic degassing and seismic amplitudes, and so involved two primary analytical tasks. The first task was to establish the variation in SO_2 emission using the OMI satellite data for a subset of volcanoes during the period from 1 October 2004 to 30 September 2010. The second task was to model seismic waveforms from all M_w 7 and larger earthquakes, from 1 January 2004 to 30 September 2010, and to estimate the PDS from surface wave amplitudes.

The subset of target volcanoes (figure 2.1) was established using several criteria: 1) to represent a global distribution, 2) to include varying tectonic regimes, and 3) where passive degassing is relatively constant and measurable with OMI. Since these volcanoes are all in an "open-vent" state, they may be more sensitive to small pressure changes from distant earthquakes. Brief descriptions of each volcano follow; all of the information, unless otherwise noted, was taken from the Smithsonian Institution Global Volcanism Program (SI GVP) (www.volcano.si.edu) volcanic activity reports, which are gathered using volcano observatory reports.

Ambrym volcano is located in Vanuatu, at 16.25°S, 168.12°E, with a summit elevation of 1334m. It erupts basalt, and has been active at least once a year during historical time. The caldera is about 12km wide, containing a lava lake that was intermittently active during the period of this study.

Bagana volcano is located in Papua New Guinea, on Bougainville Island, at 6.14°S, 155.19°E, with a summit elevation of 1750m. Viscous andesite is erupted in effusive eruptions, with little explosive activity, although pyroclastic flows accompany the occasional explosive event. A small lava dome occupies the summit crater.

Erta Ale volcano is located in Ethiopia, at 13.6°N, 40.67°E, in the Danakil depression. Its base is below sea level, and the summit elevation is 613m. The summit crater is elliptical, and contains a basaltic lava lake that has been active since at least 1967 (possibly since 1906).

Fuego volcano is located in Guatemala, at 14.47°N, 90.88°W, with a summit elevation of 3763m. It erupts basaltic to basaltic-andesite lava, with eruptive activity recorded since 1524. Fuego was continuously active during the study period, with periods of strombolian activity, passive effusion, as well as paroxysmal explosive activity (Lyons et al. 2009).

Gaua volcano is also located in Vanuatu, at 14.27°S, 167.5°E, with a summit elevation of 797m. It has a summit caldera about 6km x 9km, which erupts basaltic-to-andesitic lava. It has been active since 1962.

Merapi volcano is located on Java, in Indonesia, at 7.54°S, 110.44°E and a summit elevation of 2986m. It erupts basaltic, or basalt-andesite lava, along with pyroclastic flows and lahars.

The volcano been active since the mid-1500s, and had caused many fatalities since that time. Activity at Merapi is characterized by cycles of lava dome growth and collapse.

Pacaya volcano is also located in Guatemala, close to Fuego at 14.38°N, 90.6°W, with a summit elevation of 2552m. Activity has been essentially ongoing for several decades, with strombolian eruption of basaltic lava, as well as lava flow extrusion.

Rabaul volcano currently sits on the edge of the older Rabaul caldera, in New Britian, Papua New Guinea, at 4.27°S, 152.2°E. The summit is 688m high. Current activity is from the Tarvuvur and Vulcan vents, which produce basalt to dacite lavas.

Semeru volcano is also located on Java, in Indonesia at 8.11°S, 112.92°E. It is the highest volcano on Java, with a summit elevation of 3676m. It also erupts basaltic and basaltic-andesite lava, and has been active continuously since 1967. A lava dome is was active during the study period.

Shiveluch volcano is located on Kamchatka Peninsula, Russia, at 56.65°N, 151.36°E, with a summit elevation of 3283m. Activity during this study period was nearly continuous, with lava dome growth, ash and gas plume eruptions, pyroclastic flows, and periodic paroxysmal eruptions of andesitic lava.

Turrialba volcano is located in Costa Rica, at 10.03°N, 83.77° W, with a summit elevation of 3340m. The summit depression is 800m x 2200m, and contains three vent craters. Activity is characterized by fumerolic emission as well as strong emissions from a summit vent.

Ulawun volcano is also located in New Britian, Papua New Guinea, at 5.05°S, 151.33°E, with a summit elevation of 2334m. Typical lava composition is basaltic-andesite, with activity since 1970 that includes lava- and pyroclastic flows.

Villarrica volcano is located in central Chile, at 39.42°S, 71.93°W, with a summit elevation of 2847m. An active lava lake is sometimes present in the summit crater. The erupted lava is basalt-andesite in composition. Activity has been documented since 1558.

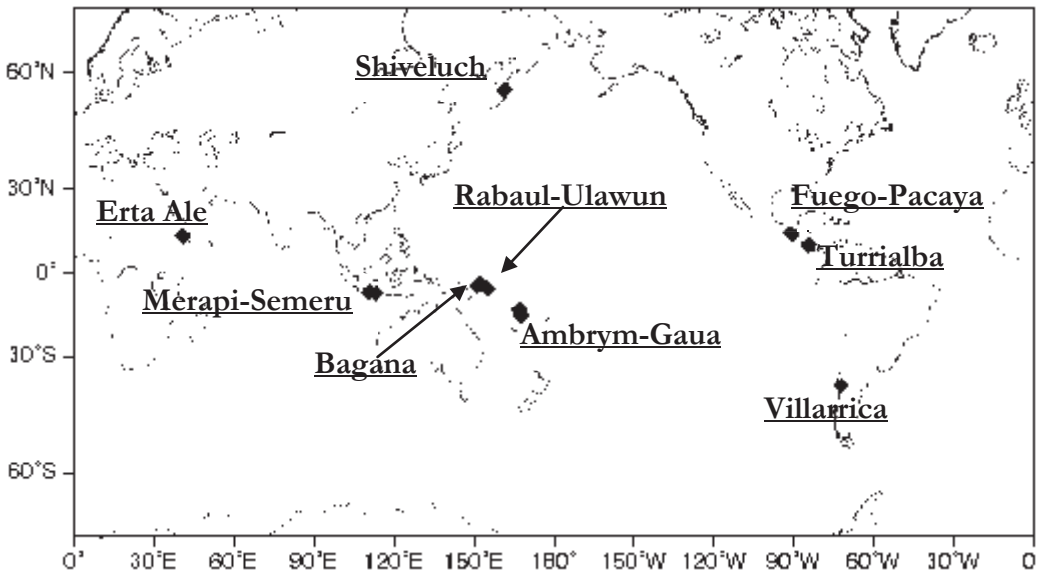

Figure 2.1. Map of target volcanoes.

2.1. SO2 Retrieval and Processing

In this study we are interested in examining subtle changes in degassing, rather than the occurrence of volcanic eruptions. Variations in volcanic SO_2 emissions are typically associated with magmatic processes in the conduit and magma chamber, and as such can be an indicator of activity at a volcano. SO_2 is released in both explosive and effusive eruptions, as well as by persistent degassing. Mechanisms involved in passive degassing involve nucleation and growth of bubbles from a supersaturated magma, and the ascent of bubbles to the surface where the gas is released to the atmosphere. These bubbles may be carried to the surface by magma convection, or by their own buoyancy (Shinohara 2008). In these systems, the rate of gas release is related to the rate of convection or gas exsolution, and ultimately linked to processes within the magmatic conduit. Satellite-based measurements provide a consistent daily measurement of SO_2, allowing these relatively small changes in SO_2 degassing to be quantified.

Following the launch of the OMI on NASA's Aura satellite in 2004, daily monitoring of volcanic SO_2 emissions became possible on a global scale (e.g., (Carn et al. 2008). The Aura satellite is in a polar orbit that crosses the equator at about 13:30 local time. OMI is a hyperspectral ultra-violet-visible (UV-VIS) imaging spectrometer that measures backscattered solar radiation in three bands. Wavelengths are measured in two bands in the UV spectrum (270-310 nm (UV1) and 310-365 (UV2)), and a third band in the visible light spectrum (365-504nm). OMI only measures during daylight hours, has a nadir footprint of 13x24km, and a swath width of 2600 km. This produces daily measurements of SO_2 for the

entire globe. The high sensitivity to lower tropospheric SO_2 and small footprint make the instrument ideal for monitoring volcanic degassing. The data collected by OMI are processed by NASA using algorithms to produce an SO_2 product file containing column densities based on four different a-priori SO_2 vertical profiles. The algorithm used to calculate SO_2 in the planetary boundary layer (PBL) is the Band Residual Difference (BRD). However, this SO_2 data was not used in this study. Instead the Linear Fit (LF) algorithm is used to determine SO_2 column density in the lower troposphere (SO_2 at 3 km altitude), the middle troposphere (8 km altitude), and the upper troposphere/lower stratosphere (17 km altitude). Corrected residuals from 10 wavelengths, calculated using the method of Yang et al, (2007), are used as input for the LF algorithm, which was developed specifically for volcanic degassing and eruptions. The algorithm adjusts total SO_2 and ozone, with a quadratic polynomial in the spectral fit, to minimize different subsets of residuals. The subsets are created by dropping the shortest wavelength bands until the 322nm band is reached, with the largest SO_2 retrieval reported as the final estimate. (Yang et al. 2007)

The raw OMI SO_2 data used in this study were processed by NASA using the operational LF algorithm (Yang et al. 2007) to produce the OMSO2 data product. The OMSO2 data were then processed using in-house software (OMIplot) (Simon Carn, personal communication, 2011). OMIplot allowed us to isolate a 2^o of latitude by 2^o of longitude box with the target volcano location in the center. SO_2 mass was then calculated within this box for each day in the study period. If two volcanoes were close enough in location that the 2^o boxes overlapped, the volcanoes were paired, and a new box was used, with edges 1^o from the edges of the volcano pairs. Table 2.1 shows the nine volcanoes or volcano pairs analyzed for this study. A daily measure of albedo that affects the accuracy of the SO_2 measurements by OMI (e.g., SO_2 emissions at low altitudes obscured by meteorological clouds) was also produced by the OMIplot software. This measure is called reflectivity, and is equivalent to the UV albedo of the total viewing area.

Table 2.1
Location of boxes used in OMIplot

Volcano	Latitude		Longitude	
	Min	Max	Min	Max
Villarrica	-40.5	-38.5	-73	-71
Merapi-Semeru	-9	-6.5	109.4	113.9
Erta Ale	12.6	14.6	39.6	41.6
Ambrym-Gaua	-17.2	-13.2	166	169
Bagana	-7	-5	154	156
Fuego-Pacaya	13.5	15.5	-91.8	-89.8
Rabaul-Ulawun	-6	-3.2	150.3	153.2
Turrialba	9	11	-84.7	-82.7
Shiveluch	55.6	57.6	160.3	162.3

The daily SO_2 masses calculated with OMIplot were then analyzed using Matlab software. The data were smoothed using continuous one week averaging so that each daily value was the average of the SO_2 mass from that day and the six days prior to that day. This smoothing reduces the effect of noise and atmospheric conditions. Reflectivity data were also smoothed using a similar algorithm, but using a 14 day continuous average.

2.2. Earthquake Modeling and Peak Dynamic Stress Calculations

Most previous studies of the triggering of volcanic activity by earthquakes use simple distance and magnitude criteria to relate earthquakes to eruptions. In order to more accurately quantify the effect of earthquakes capable of triggering changes at distant volcanoes, we modeled the PDS from each earthquake at each volcano using synthetic surface waves. This approach allowed us to incorporate both the radiation pattern and distance into the assessment of the effect of an earthquake on volcanic systems. It also allowed us to investigate the effect of varying levels of PDS on activity. Surface wave amplitudes were modeled for events in the global USGS earthquake catalog (table A.1) chosen using the following criteria: occurrence date from 1 January 2004 to 30 September 2010; $M_w \geq 7$; and depth $\leq$ 35km. In addition, all events of $M_w \geq 8$ during the study period were included, regardless of depth. The rationale for the use of magnitude and depth criteria is that only large, shallow earthquakes produce high amplitude surface waves capable of transmitting dynamic stress over many thousands of kilometers.

A suite of computational programs, Computer Programs in Seismology (CPS) (Herrmann 2002), was used to model surface wave amplitudes. This program produces synthetic seismograms based on a layered Earth velocity model, the focal mechanism, depth and moment magnitude of the earthquake, as well as the distance and azimuth of the test location from the earthquake. The layered Earth model used here is AK135-F (figure A.1), which details the thickness, seismic wave velocity, density, and Q value for each layer in the Earth. The Q value is a measure of attenuation. The Earth model is the basis for how seismic waves travel through each layer of the earth. The focal mechanism of the earthquake provides information on the geometry of the ruptured fault, which, along with the depth constraint, determines the radiation pattern of the seismic waves. The magnitude is related to the amount of energy released by the earthquake.

The program was tested using five earthquakes from the catalog established for this study, and real data from the Incorporated Research Institutions for Seismology (IRIS) Data Management Center. Synthetic seismograms were produced to compare with the real data, using CPS and the location of each seismograph recording the real data for the test earthquakes. The synthetics were then compared to the real seismograms to determine the level of accuracy of the synthetics. Hill (2008) found that the occurrence of earthquakes

triggered by large distant earthquakes typically began with the arrival of the Love and Rayleigh waves at periods from 15-30 seconds, so we focused on surface waves within that range. The seismograms, both real and synthetic, were filtered between .02Hz and .49Hz and then examined in the window between the arrival times of the 30s period and 20s period for both Love and Rayleigh waves. The window of analysis was chosen because the 30 second to 20 second period range is within the flat response of the seismometers that provided the real data used in the testing, as well as being a range of high amplitude surface waves at many distances. Of interest was the maximum ground velocity amplitude in those windows. The synthetic seismograms that the PDS calculations were based on provided a reasonable estimation for the maximum amplitude of ground velocity at each volcano for any given earthquake in the catalog.

The results of testing the CPS program suite showed that the amplitude of the synthetic seismogram in the chosen window of surface wave arrivals was typically no more than 5 times the amplitude of the real seismogram (figure 2.2). The same is true when the inverse is considered, i.e. the amplitude of the real seismogram is compared to the amplitude of the synthetic seismogram. The amplitude ratio of the vertical and transverse seismograms exceeded 5 for only 12% of the tested stations, while the radial seismogram amplitude ratio exceeded 5 for 22% of the tested stations. The mean synthetic:real vertical seismogram amplitude ratio is 2.8, with a standard deviation of 3.1. For the synthetic:real radial seismogram amplitude ratios the mean is 2.7, with a standard deviation of 2.2. The transverse synthetic:real seismogram amplitude ratio has a mean of 2.2, with a standard deviation of 2.6.

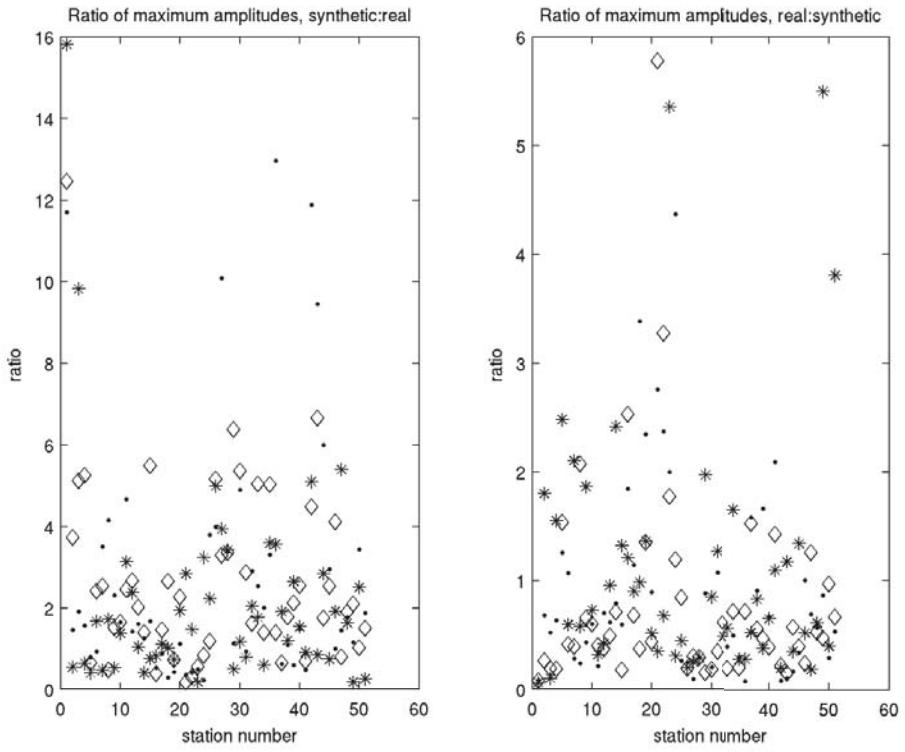

Figure 2.2. CPS test results. Ratio of maximum surface wave amplitudes of real and synthetic seismograms. Dots (.), diamonds (◊), and asterisks (*) indicate the amplitude ratio for vertical, radial, and transverse traces, respectively.

In a careful analysis of surface wave modeling errors for real and synthetic data along similar great circle paths van der Lee (1998) found similar levels of misfits. In that study, uncertainties in source processes and near-source structure were implicated in the majority of the misfit. So, while our modeling was relatively simple and did not account for finite fault complexity (e.g., directivity), we do not feel a more sophisticated modeling procedure would significantly improve the discrepancy in amplitudes between the synthetic and real seismograms.

Once the synthetics were established as a reasonable estimate for the amplitude of the surface waves, synthetic seismograms were created for each earthquake, using the locations of each volcano in the catalog as the receivers. These synthetic seismograms (figure 2.3) were the basis for the PDS calculations.

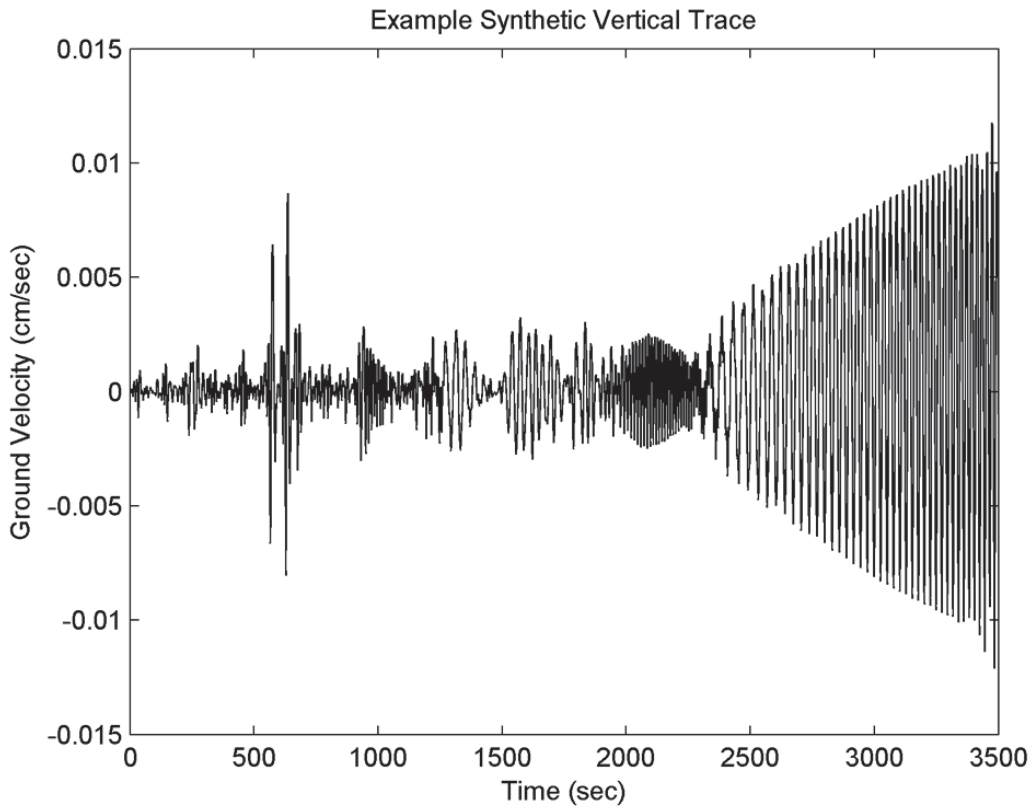

Figure 2.3. A vertical trace synthetic seismogram produced by the CPS program suite for a M_w 7.5 earthquake on 11 November 2004 in Indonesia, recorded 163 degrees away at Villarrica (Chile).

The PDS was calculated following the method of Velasco et al, (2004) where PDS = $\nu(\mu/\beta)$. The east, north, and vertical components of each synthetic seismogram were combined into a single velocity vector, from which a peak velocity (ν) was derived for both Love and Rayleigh waves. The arrival times of the 30s period and 20s period surface waves was calculated using the distance between the epicenter of each earthquake and each volcano and the average velocity of the Love and Rayleigh waves. Note that these estimates are most appropriate for Love waves, which are dominated by shear waves. The PDS calculation is less accurate for Rayleigh waves, however it is still a useful measure for comparison. These arrival times defined the edges of the surface wave arrival windows, and the maximum amplitude within that window was used to calculate PDS. Average crustal values of 3.3 x 10^{10} Pa for rigidity (μ), and 3.5 km/sec for shear wave velocity (β) were used for these calculations (Velasco et al. 2004). The result of those calculations was a PDS for Love waves and Rayleigh waves for each earthquake at each volcano location

2.3. SO_2 Time Series Analysis

We used two techniques to compare the earthquake data with the OMI-derived SO_2 mass time series for each volcano. The first method involved identifying periods of elevated SO_2 emission and searching for a prior triggering earthquake. The second method used the earthquake catalog, sorted for various levels of PDS, and examined the coincident SO_2 emission time series for evidence of elevated emissions that may have been triggered by the earthquake.

2.3.1. Comparison of periods of elevated SO2 emission with prior earthquakes

The first step was to establish a time-averaged baseline value for SO_2 degassing for each volcano or volcano pair. For the purposes of this paper, volcano pairs will be referred to by hyphenating the two names, and treated as one. The SI GVP activity reports in conjunction with thermal alerts derived from the Moderate Resolution Imaging Spectroradiometer (MODIS) (Wright et al. 2004) were used to identify periods of above average activity. The periods of 'average' activity were then isolated from the entire SO_2 time series. That subset of SO_2 values for average activity was further refined using the smoothed reflectivity values for each analysis region. In order to avoid underestimating SO_2 emission, a reflectivity threshold for each volcano was established, above which significant masking of volcanic SO_2 by meteorlogical clouds was deemed likely (Carn 2008). SO_2 values within periods of average activity when reflectivity was below the established reflectivity threshold were then averaged to determine a baseline daily degassing SO_2 value for each volcano or volcano pair.

These baseline calculations involved a number of sources of error. A "row anomaly", believed to be due to an obstruction in the instrument field-of-view (FOV), began to affect OMI in late August 2008, and steadily worsened through early 2010. The row anomaly creates a stripe of bad data values that affected some of the retrieval values, if the location of the volcano fell in the anomaly stripe on any given day. The true SO_2 value cannot be retrieved from the values recorded within the row anomaly. These anomalous data points were replaced with zeros (0) by the OMIplot processing software in the analysis. The smoothed SO_2 mass dataset includes these zero values, and so, potentially, could the baseline SO_2 value. In this case the baseline would be lower than actual. An interpolation of SO_2 values from adjacent unaffected pixels could minimize the effect of this row anomaly.

Reflectivity also plays a role in the accuracy of the SO_2 measurements. When reflectivity is high the retrieved SO_2 mass is usually lower, due to the masking of low altitude SO_2 by meteorological clouds. We attempted to account for this effect by only including days with a reflectivity lower than the reflectivity threshold in the SO_2 mass calculations.

The assumed altitude of the volcanic plume also affects the SO_2 retrieval. OMI records the UV radiance backscattered by the Earth's atmosphere at the "top-of-the-atmosphere" (TOA). The LF algorithm uses this TOA radiance measurement to retrieve the total SO_2

column amount, but requires an assumption of the SO_2 vertical profile to correctly account for SO_2 absorption and Rayleigh scattering (Yang et al. 2009). The LF algorithm is designed to take the SO_2 plume height into account in calculations, however, if the height is poorly constrained due to a lack of data or monitoring, the retrieved SO_2 column (and derived SO_2 mass) will contain some error (Yang et al. 2007). Factors that could be considered to minimize this error are wind speed at various atmospheric levels, as well as information from other remote sensing instruments that can provide reasonable constraints on plume height. In this study, plumes with a reported altitude in the SI GVP catalog were analyzed at the reported altitude. All other data was analyzed at the 3 km level under the assumption that passively degassed SO_2 would rise no higher than 3-4 km at the selected volcanoes.

Another complication of accurate assignment of SO_2 emissions to a specific volcano is the effect of degassing or eruptions by nearby volcanoes. The SO_2 released into the atmosphere from other sources can drift so that it is located within the area of the volcanoes included in this study. The aim was to select an analysis box size small enough to minimize this effect, while still containing all active vents of each volcano and including enough OMI pixels to be a reasonable measurement. When large eruptions were reported at nearby volcanoes and the plume was seen to drift across the area of a study volcano, the SO_2 mass for the impacted days was not included in baseline SO_2 calculations. This only happened twice during the study period: Soufriere Hills (Monserrat) erupted on 24 May 2006 and influenced the SO_2 data for Turrialba, and Santa Ana (El Salvador) erupted on 1 October 2005, affecting the SO_2 data for Fuego-Pacaya.

Additionally, because the level of activity at each volcano was determined using the monthly summary activity reports from the SI GVP, which are, in general, qualitative, uncertainty exists in the assignation of above-average activity and average activity time periods for each volcano. The SO_2 baseline rates were established by using the SO_2 emission data for periods of time with average activity, therefore the accuracy in determining activity can affect the accuracy of the baseline.

Periods of above-average activity for each volcano or volcano pair were identified using the baseline SO_2 degassing value. When an SO_2 mass exceeding a value equal to twice the baseline level was observed in the full time series dataset for that volcano, the event was considered a response if it lasted more than 6 days, and was separated by at least three days from an adjacent response. The 6-day response time was chosen to ensure that the increase in SO_2 was indicative of a true response. The 3-day separation between responses ensured that the measured SO_2 mass was not an artifact of lingering atmospheric SO_2 from previous increases in degassing. The delay time between each response and all earthquakes that occurred before the response start date was calculated. In addition, the earthquake dataset was filtered using a PDS threshold of 10 kPa, and the delay time between each response and those earthquakes that met the threshold requirement was calculated. The delay times were analyzed for individual volcanoes and results for all volcanoes were combined into a single

dataset. This was repeated using a random catalog of earthquakes to determine if the association with our selected earthquake catalog (table A.1) was significant.

2.3.2. Comparison of earthquakes with pre-event and post-event SO2 emission

The second analysis of the SO_2 time series followed the method of Delle Donne et al (2010), and examined each volcano separately. The SO_2 mass was averaged in two 14-day windows, one immediately preceding each earthquake, and the other immediately following each earthquake in the catalog. The window following the earthquake included the day of the earthquake itself. Then the ratio of post-earthquake average SO_2 mass to pre-earthquake average SO_2 mass was calculated. The relationship between earthquake occurrence and the ratios of post-earthquake to pre-earthquake SO_2 emissions were evaluated with minimum thresholds of 1.2 to 2.0, increasing by increments of 0.2. The number of times that the average SO_2 following an earthquake met the ratio threshold criteria was recorded, as well as the number of times the average SO_2 was higher (by the same ratio threshold criteria) in the window preceding the earthquake. This calculation was repeated using increasing levels of PDS, from 5 kPa to 100 kPa, to filter the earthquake catalog and investigate the significance of higher levels of dynamic stress. The same reflectivity threshold used in the baseline calculations was used here to minimize atmospheric influence on the data. Within the pre- and post-earthquake windows, only days with a reflectivity value less than the threshold were considered. If there were fewer than 8 days meeting the reflectivity criteria in either window for an earthquake, that earthquake was not considered in the analysis. Figure 2.4 illustrates the windowing method.

In order to compare the occurrence of positive responses to an earthquake trigger to a coincidental occurrence, we used the same windowing method for each day of the study period. This, in effect, is analyzing the SO_2 time series as if there were an earthquake every day that could affect SO_2 emissions. The results of this analysis allowed us to determine if there was a notable deviation in occurrence of positive response in association with a real earthquake from that expected from random coincidence.

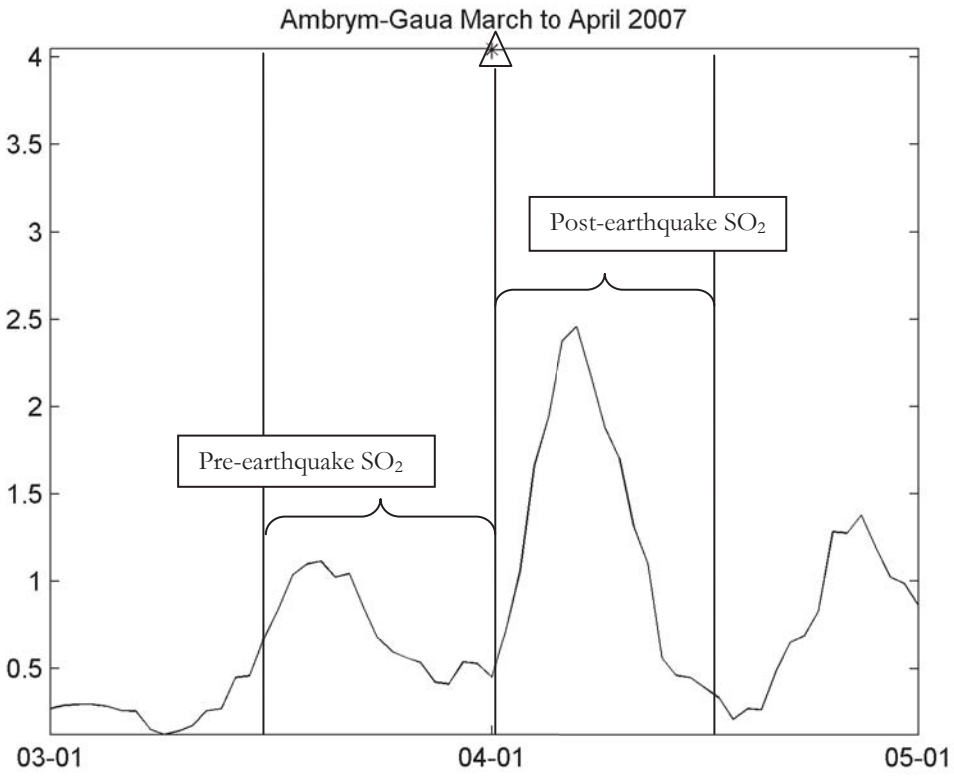

Figure 2.4: Example of pre- and post-earthquake window analysis using an SO_2 time series from Ambrym-Gaua, from 1 March 2007 through 1 May 2007. This time period includes a M_w 8.1 earthquake that occurred on 1 April 2007 in the Solomon Is., (highlighted by the triangle and center vertical line). The outer vertical lines represent the edges of the 14-day window in which daily SO_2 was averaged.

3. Results

3.1. SO_2 Baseline Calculations

With the exception of Fuego-Pacaya and Shiveluch, the baseline SO_2 calculations (table 3.1) yielded a minimum threshold that was used to investigate periods of time when the volcano exhibited above-average levels of degassing, even in the absence of other signs of activity (MODIS thermal alerts, plume reports, etc). In table 3.1, the 'number of days included' column indicates the total number of days that met the criteria for average activity and below-threshold reflectivity for each volcano. Standard deviation of SO_2 mass and reflectivity threshold is also noted for each volcano

Table 3.1:
SO_2 baseline values for each volcano or volcano pair.

Volcano Name	SO_2 Baseline (kT)	Standard Deviation (kT)	# of days included	Reflectivity Threshold
Ambrym-Gaua	1.7673	.5072	865	35%
Bagana	.0344	.0303	596	35%
Erta Ale	.0018	.0004	1824	20%
Fuego-Pacaya	.0049	N/A	26	30%
Merapi-Semeru	.0706	.0279	1514	35%
Rabaul-Ulawun	.0094	.0161	531	35%
Turrialba	.0041	.0029	732	40%
Villarrica	.0062	.0031	643	30%
Shiveluch	N/A	N/A	N/A	40%

The baseline analysis for both Fuego-Pacaya and Shiveluch was unsuccessful primarily because of the continuous high level of reported activity at these volcanoes. The analysis for Fuego-Pacaya yielded only 26 days that met reflectivity and activity criteria. For this reason, the baseline SO_2 is not very reliable. Similarly, Shiveluch had no reported days of inactivity during the study period that also met the reflectivity criteria, and subsequently no baseline SO_2 could be calculated. In both of these cases, but particularly for Shiveluch, very detailed reporting of activity would be necessary for this method to produce a reliable baseline SO_2. In addition, the high latitude location of Shiveluch means that OMI's row anomaly affected a larger number of pixels in the swath (since the anomaly is latitude dependant). With these limitations on the SO_2 emission data, Fuego-Pacaya and Shiveluch have been excluded from

our baseline and delay time analysis, and Shiveluch has also been excluded from the pre-and post-earthquake window analysis.

Figure 3.1 shows an example of a calculated SO_2 baseline overlain on a full SO_2 time series for Villarrica volcano. Similar plots for all volcanoes are provided in Appendix A. The lower line is the SO_2 baseline, and the upper line indicates the baseline + 2σ. The standard deviation represents the variability of SO_2 mass values used to calculate the baseline. Periods of time when SO_2 emission exceeds the baseline are considered above average activity.

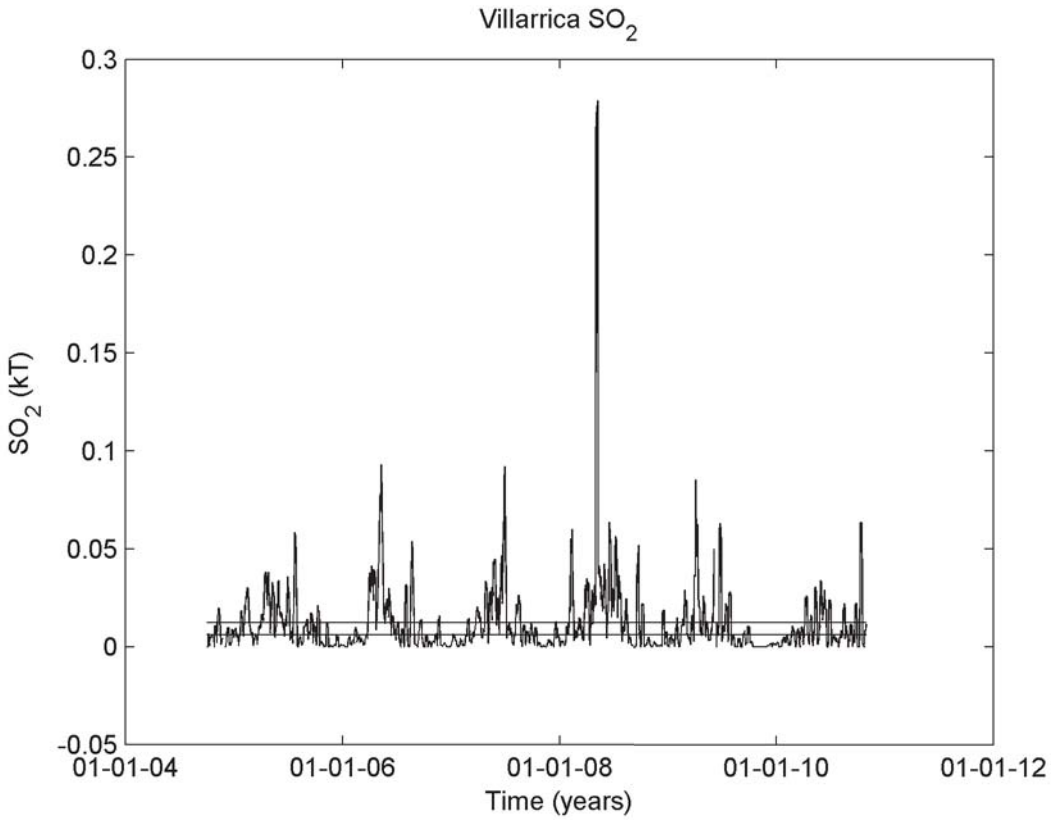

Figure 3.1. OMI-derived SO_2 time series for Villarrica, with baseline degassing thresholds indicated. The lower line is the calculated baseline, and the upper line is the 2σ threshold.

3.2. Peak Dynamic Stress (PDS)

The PDS values, which include the effects of distance and seismic radiation pattern from the source, contain more useful information than moment magnitude alone. The significance of including these parameters is apparent when PDS is plotted against moment magnitude (figure 3.2); we can identify numerous instances where the PDS generated by an earthquake of smaller magnitude is higher for specific volcanoes than the PDS generated by an

earthquake of larger magnitude. Most notably, a M_w 7.3 generated a PDS higher than all other earthquakes up to M_w 8.0. If the earthquake catalog was filtered based on magnitude alone these smaller earthquakes might be removed from consideration. The PDS values provided the criterion for filtering the earthquake catalog in the subsequent analysis of variations in the SO_2 time series for each volcano in the study.

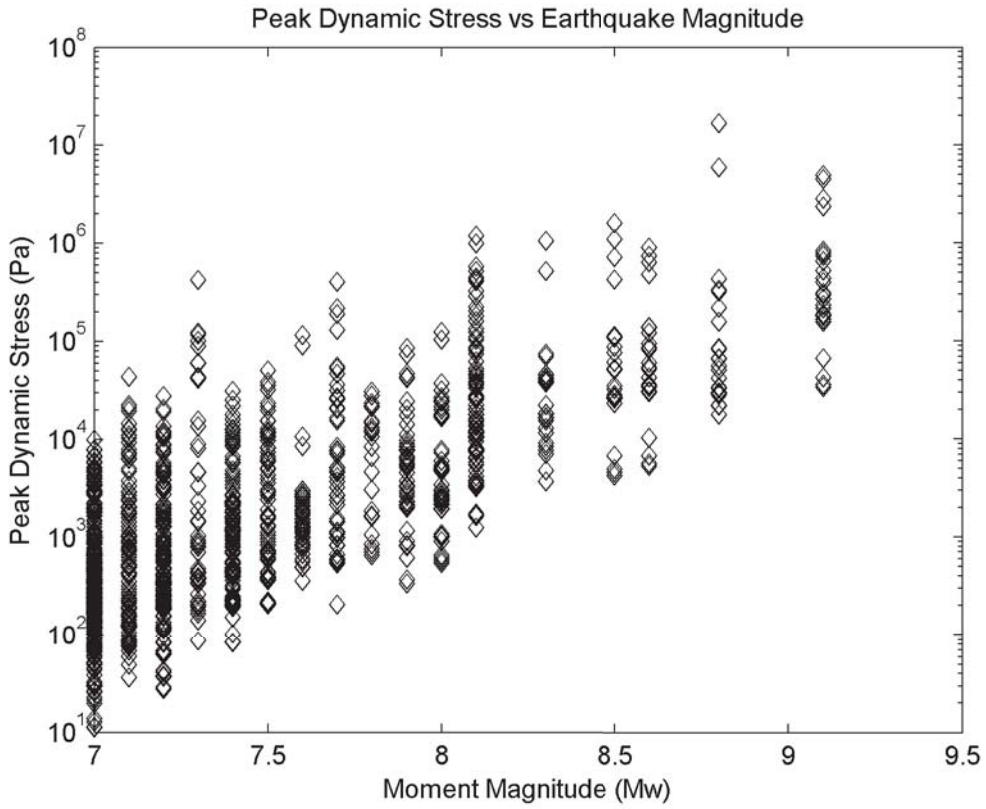

Figure 3.2. Comparison of PDS and moment magnitude for all modeled earthquakes at all volcanoes.

3.3. Delay Time Analysis

The results of the delay time and SO_2 response analysis were inconclusive. The distribution of delay times between the origin time of an earthquake and a positive SO_2 response does not indicate a pattern of triggering by earthquakes generating at least 10 kPa PDS. Delay times showed a mode of 20 to 24 days (figure 3.3). However, when a random catalog of earthquakes is generated with the same 10 kPa PDS criterion, the distribution indicates a higher number of occurrences of less than 15 days between earthquake origin time and SO_2 response (figure 3.4) than the real earthquake catalog. This analysis was repeated using varied PDS threshold criteria and maximum delay time. No combination of criteria yielded a

clear indication of correlation between earthquakes and SO_2 response beyond random coincidence. These results prompted a different method of analysis.

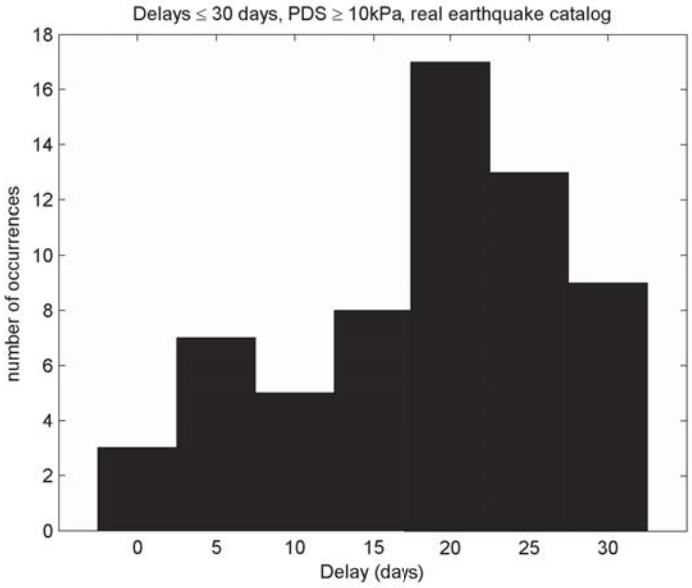

Figure 3.3. Histogram of delay times ≤30 days between SO_2 response and real earthquakes meeting the 10 kPa PDS criteria.

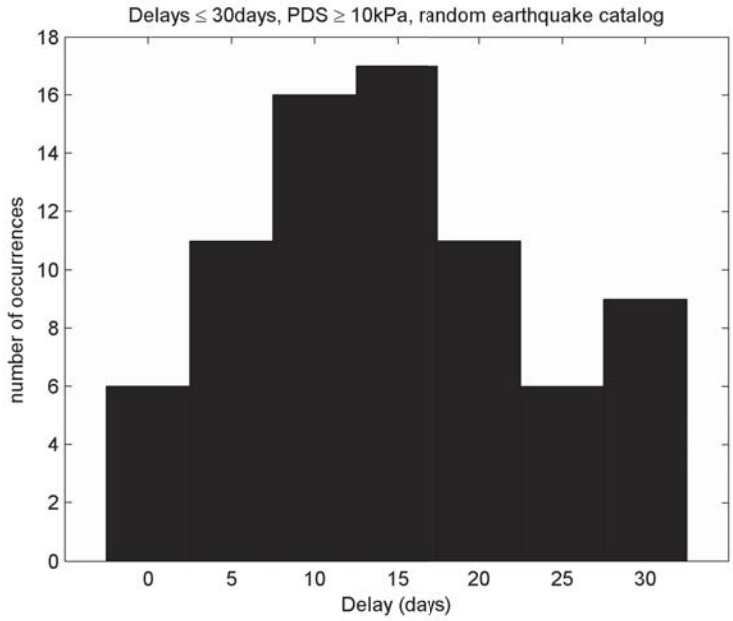

Figure 3.4. Histogram of delay times ≤30 days between SO_2 response and randomly generated earthquakes.

3.4. Pre- and Post-Earthquake Window Analysis

The results of analyzing average SO_2 emission within pre- and post-earthquake time periods, detailed below, suggest that the style of eruption of a volcano may play a primary role in whether earthquake generated dynamic stress influences SO_2 degassing. Volcanoes that exhibit very open vent activity such as active lava lakes during the period of this study appear to be susceptible to stress-triggered increases in activity, while those undergoing dome-building, or with less open-vent activity are not notably influenced by dynamic stresses. The results from each of the volcanoes, or volcano pairs, are detailed in the following sections. Note that the results from all tested levels of PDS are presented, however, if the number of qualifying earthquakes was fewer than 3 the subset is deemed to be too small for a definitive connection to be drawn between occurrence of positive SO_2 response and earthquake generated PDS.

3.4.1. Ambrym-Gaua

The results of the windowing analysis for Ambrym-Gaua (table 3.2) show that this volcano pair exhibits an apparent response of increased SO_2 emissions after an earthquake at all levels of PDS analyzed. At the minimum threshold of 5kPa for earthquakes, 16 earthquakes met the criteria, and post-earthquake SO_2 was at least 1.2 times higher than the pre-earthquake SO_2 for 63%, or 10, of those earthquakes. According to the analysis of the full SO_2 time series, it is expected that the SO_2 emissions will be higher for any given day 41% of the time (i.e., a random occurrence) and higher before any given day 35% of the time. Given that there are 16 earthquakes in the subset catalog for this analysis, random occurrence would predict that pre-earthquake SO_2 emissions would be higher on ~6 occasions and post-earthquake SO_2 emissions would be higher on ~5 occasions. However, the results show that 10 times out of 19 the SO_2 was higher after an earthquake, and only once was it higher before the earthquake. This is a clear indication that surface waves from an earthquake producing at least 5 kPa PDS will trigger a response in either Ambrym, Gaua, or both together. At the highest PDS level, 100 kPa, there are still five earthquakes that meet the criteria of both reflectivity and PDS. At this level, 80% of those five earthquakes are associated with an increase in SO_2 immediately following the passage of the surface waves.

Table 3.2:
Comparison of pre- and post-earthquake SO_2 emission for Ambrym-Gaua. The post-earthquake values indicate the number of times SO_2 is higher after the earthquake, pre values indicate the number of times SO_2 is higher before the earthquake.

[1] PDS = 0 indicates that no earthquake were considered; in other words the ratio was computed for ever possible pair of adjacent 14-day windows.
[2] This is the number of days meeting reflectivity criteria for full time series window analysis.

		Percentage of total occurrences when the SO_2 ratio exceeds threshold					
PDS threshold (Pa)		**Ratio ≥ 1.2**	**Ratio ≥ 1.4**	**Ratio ≥ 1.6**	**Ratio ≥ 1.8**	**Ratio ≥ 2**	**# of earthquakes**
0[1]	Post	41%	31%	24%	19%	13%	1561[2]
	Pre	35%	27%	19%	14%	10%	
5000	Post	63%	56%	50%	31%	25%	16
	Pre	6%	6%	6%	6%	6%	
10000	Post	62%	54%	46%	31%	23%	13
	Pre	8%	8%	8%	8%	0%	
25000	Post	55%	45%	36%	18%	9%	11
	Pre	9%	9%	9%	9%	0%	
50000	Post	56%	56%	44%	22%	11%	9
	Pre	11%	11%	11%	11%	0%	
75000	Post	56%	56%	44%	22%	11%	9
	Pre	11%	11%	11%	11%	0%	
100000	Post	80%	80%	60%	40%	20%	5
	Pre	20%	20%	20%	20%	0%	

3.4.2. Erta Ale

Erta Ale (table 3.3), like Ambrym-Gaua, shows a higher frequency of post-earthquake elevated SO_2 response than expected from analysis of the SO_2 time series alone. At Erta Ale, 12 earthquakes produce at least 5kPa PDS, and of those, 58% coincide with an elevated SO_2 in the window after the earthquake, while the expected frequency is 42% from the full time series analysis. Additionally, the number of times SO_2 is higher prior to an earthquake is less than expected from the expected values. This pattern is visible as the PDS threshold is increased.

Table 3.3:
Comparison of pre- and post-earthquake SO_2 emission for Erta Ale.

See Table 3.2 for details.

		Percentage of total occurrences when the SO_2 ratio exceeds threshold					
PDS threshold (Pa)		**Ratio ≥ 1.2**	**Ratio ≥ 1.4**	**Ratio ≥ 1.6**	**Ratio ≥ 1.8**	**Ratio ≥ 2**	**# of earthquakes**
0[1]	Post	42%	36%	32%	30%	28%	2054[2]
	Pre	44%	39%	35%	32%	29%	
5000	Post	58%	58%	58%	58%	58%	12
	Pre	25%	25%	17%	17%	17%	
10000	Post	75%	75%	75%	75%	75%	8
	Pre	25%	25%	25%	25%	25%	
25000	Post	100%	100%	100%	100%	100%	4
	Pre	0%	0%	0%	0%	0%	
50000	Post	100%	100%	100%	100%	100%	4
	Pre	0%	0%	0%	0%	0%	
75000	Post	100%	100%	100%	100%	100%	3
	Pre	0%	0%	0%	0%	0%	
100000	Post	100%	100%	100%	100%	100%	2
	Pre	0%	0%	0%	0%	0%	

3.4.3. Turrialba

The earthquake analysis at Turrialba (table 3.4) indicates that the occurrence of increased SO_2 after an earthquake is notable at all levels of PDS. However, the number of qualifying earthquakes is low except at the 5kPa level. Of the five earthquakes that met the PDS criteria 60% occur when post-earthquake SO_2 is higher than pre-earthquake SO_2, an increase over the expected occurrence of 47%. This holds true for all SO_2 ratio thresholds. Likewise, the number of occurrences of higher SO_2 pre-earthquake is less than expected for all SO_2 ratio thresholds.

Table 3.4:
Comparison of pre- and post-earthquake SO_2 emission for Turrialba.

See Table 3.2 for details.

		Percentage of total occurrences when the SO_2 ratio exceeds threshold					
PDS threshold (Pa)		**Ratio ≥ 1.2**	**Ratio ≥ 1.4**	**Ratio ≥ 1.6**	**Ratio ≥ 1.8**	**Ratio ≥ 2**	**# of earthquakes**
0[1]	Post	47%	37%	31%	25%	19%	418[2]
	Pre	32%	22%	17%	10%	6%	
5000	Post	60%	60%	60%	40%	40%	5
	Pre	20%	20%	0%	0%	0%	
10000	Post	50%	50%	50%	50%	50%	2
	Pre	0%	0%	0%	0%	0%	
25000	Post	50%	50%	50%	50%	50%	2
	Pre	0%	0%	0%	0%	0%	
50000	Post	100%	100%	100%	100%	100%	1
	Pre	0%	0%	0%	0%	0%	
75000	Post	100%	100%	100%	100%	100%	1
	Pre	0%	0%	0%	0%	0%	
100000	Post	100%	100%	100%	100%	100%	1
	Pre	0%	0%	0%	0%	0%	

3.4.4. Villarrica

At Villarrica (table 3.5), earthquakes generating a PDS up to 25 kPa appear to trigger increased SO_2 emissions, primarily at the SO_2 ratio threshold of 1.2. For the seven earthquakes generating 5 kPa, 57% correlate with an increase of SO_2 post-event, a slight increase over what was expected. However, only 14% occur with higher pre-earthquake SO_2. At the 25 kPa PDS level the occurrence (75%) is much higher than expected (54%) for post-earthquake SO_2.

Table 3.5:
Comparison of pre- and post-earthquake SO_2 emission for Villarrica.

See Table 3.2 for details.

		Percentage of total occurrences when the SO_2 ratio exceeds threshold					
PDS threshold (Pa)		**Ratio ≥ 1.2**	**Ratio ≥ 1.4**	**Ratio ≥ 1.6**	**Ratio ≥ 1.8**	**Ratio ≥ 2**	**# of earthquakes**
0[1]	Post	54%	46%	40%	35%	29%	1038[2]
	Pre	32%	26%	23%	20%	17%	
5000	Post	57%	43%	28%	14%	0%	7
	Pre	14%	14%	14%	14%	14%	
10000	Post	75%	75%	50%	25%	0%	4
	Pre	0%	0%	0%	0%	0%	
25000	Post	75%	75%	50%	25%	0%	4
	Pre	0%	0%	0%	0%	0%	
50000	Post	50%	50%	50%	0%	0%	2
	Pre	0%	0%	0%	0%	0%	
75000	Post	50%	50%	50%	0%	0%	2
	Pre	0%	0%	0%	0%	0%	
100000	Post	50%	50%	50%	0%	0%	2
	Pre	0%	0%	0%	0%	0%	

3.4.5. Fuego-Pacaya

Fugeo-Pacaya shows a greater occurrence of higher pre-earthquake SO_2 than expected at all levels of PDS and SO_2 ratio thresholds, as well as fewer occurrences of higher post-earthquake SO_2 than expected at all levels, perhaps indicating that dynamic stresses result in subdued emission. Of the 13 earthquakes that met the criteria for 5 kPa PDS 77% were associated with higher pre-earthquake SO_2 while only 15% were associated with higher post-earthquake SO_2 at the ratio threshold of 1.2. The expected occurrence from the full SO_2 time series analysis was 38% for higher post-earthquake SO_2 and 44% for pre-earthquake SO_2.

Table 3.6:
Comparison of pre- and post-earthquake SO_2 emission for Fuego-Pacaya.

See Table 3.2 for details.

		Percentage of total occurrences when the SO_2 ratio exceeds threshold					
PDS threshold (Pa)		**Ratio ≥ 1.2**	**Ratio ≥ 1.4**	**Ratio ≥ 1.6**	**Ratio ≥ 1.8**	**Ratio ≥ 2**	**# of earthquakes**
0[1]	Post	38%	31%	26%	23%	21%	1565[2]
	Pre	44%	37%	30%	24%	29%	
5000	Post	15%	15%	15%	8%	8%	13
	Pre	77%	62%	54%	54%	54%	
10000	Post	20%	20%	20%	10%	10%	10
	Pre	80%	60%	50%	50%	50%	
25000	Post	20%	20%	20%	20%	20%	5
	Pre	80%	40%	40%	40%	40%	
50000	Post	33%	33%	33%	0%	0%	3
	Pre	67%	33%	33%	33%	33%	
75000	Post	33%	33%	33%	0%	0%	3
	Pre	67%	33%	33%	33%	33%	
100000	Post	33%	33%	33%	0%	0%	3
	Pre	67%	33%	33%	33%	33%	

3.4.6. Bagana

Like Fuego-Pacaya, the results of the SO_2 time series and earthquake window analysis for Bagana (table 3.7) show fewer occurrences of increased SO_2 emissions following an earthquake than expected from the full SO_2 analysis. The occurrence of an increased SO_2 output prior to an earthquake is also lower than what is expected for some cases. At the SO_2 ratio threshold of 1.2, in particular, the occurrence of elevated SO_2 post-earthquake is only 12% at the 25 kPa PDS level compared to an expected occurrence of 39%. Conversely, the occurrence of elevated SO_2 pre-earthquake is 63%, much higher than the expected 42%.

Table 3.7:
Comparison of pre- and post-earthquake SO_2 emission for Bagana.

See Table 3.2 for details.

		Percentage of total occurrences when the SO_2 ratio exceeds threshold					
PDS threshold (Pa)		**Ratio ≥ 1.2**	**Ratio ≥ 1.4**	**Ratio ≥ 1.6**	**Ratio ≥ 1.8**	**Ratio ≥ 2**	**# of earthquakes**
0[1]	Post	39%	31%	23%	18%	16%	763[2]
	Pre	42%	36%	31%	27%	24%	
5000	Post	20%	10%	10%	10%	10%	10
	Pre	60%	60%	30%	30%	30%	
10000	Post	22%	11%	11%	11%	11%	9
	Pre	56%	56%	33%	33%	33%	
25000	Post	12%	0%	0%	0%	0%	8
	Pre	63%	63%	38%	38%	38%	
50000	Post	17%	0%	0%	0%	0%	6
	Pre	50%	50%	33%	33%	33%	
75000	Post	20%	0%	0%	0%	0%	5
	Pre	40%	40%	20%	20%	20%	
100000	Post	20%	0%	0%	0%	0%	5
	Pre	40%	40%	20%	20%	20%	

3.4.7. Merapi-Semeru

Merapi-Semeru, like Fuego-Pacaya and Bagana, shows a greater occurrence of elevated SO_2 pre-earthquake than expected, at all levels of PDS and SO_2 ratio thresholds. The number of earthquakes meeting the 50 kPa-100kPa criteria is too few, however, for a valid analysis. When a PDS level of 25 kPa is considered, even at the SO_2 ratio threshold of 1.2 there are no occurrences of elevated SO_2 post-earthquake, as compared to the expected occurrence of 33%. Additionally, at this PDS level, 85% of the qualifying earthquakes are associated with elevated SO_2 pre-earthquake when the expected occurrence is 44%.

Table 3.8:
Comparison of pre- and post-earthquake SO_2 emission for Merapi-Semeru.

See Table 3.2 for details.

		Percentage of total occurrences when the SO_2 ratio exceeds threshold					
PDS threshold (Pa)		**Ratio ≥ 1.2**	**Ratio ≥ 1.4**	**Ratio ≥ 1.6**	**Ratio ≥ 1.8**	**Ratio ≥ 2**	**# of earthquakes**
0[1]	Post	33%	24%	18%	14%	11%	1492[2]
	Pre	44%	34%	26%	20%	17%	
5000	Post	14%	14%	14%	7%	7%	14
	Pre	71%	57%	43%	43%	36%	
10000	Post	18%	18%	18%	9%	9%	11
	Pre	73%	64%	45%	45%	36%	
25000	Post	0%	0%	0%	0%	0%	7
	Pre	85%	71%	43%	43%	43%	
50000	Post	0%	0%	0%	0%	0%	3
	Pre	67%	67%	67%	67%	67%	
75000	Post	0%	0%	0%	0%	0%	3
	Pre	67%	67%	67%	67%	67%	
100000	Post	0%	0%	0%	0%	0%	2
	Pre	50%	50%	50%	50%	50%	

3.4.8. Rabaul - Ulawun

The analysis of the full SO_2 time series for Rabaul-Ulawun (table 3.9) indicates that there should be slightly fewer occurrences of elevated SO_2 post-earthquake than pre-earthquake. However the results show that while this is indeed the case, the overall occurrence is much less than expected from the full SO_2 time series analysis at all levels of PDS and SO_2 ratio thresholds. Elevated SO_2 post-earthquake at the 5 kPa level occurs for just one of the nine qualifying earthquake, while the occurrence of pre-earthquake elevated SO_2 is only 22%.

Table 3.9:
Comparison of pre- and post-earthquake SO_2 emission for Rabaul-Ulawun.

See Table 3.2 for details.

		Percentage of total occurrences when the SO_2 ratio exceeds threshold					
PDS threshold (Pa)		**Ratio ≥ 1.2**	**Ratio ≥ 1.4**	**Ratio ≥ 1.6**	**Ratio ≥ 1.8**	**Ratio ≥ 2**	**# of earthquakes**
0[1]	Post	32%	24%	19%	14%	11%	838[2]
	Pre	43%	34%	27%	22%	20%	
5000	Post	11%	11%	11%	11%	11%	9
	Pre	22%	22%	11%	11%	0%	
10000	Post	14%	14%	14%	14%	14%	7
	Pre	14%	14%	14%	14%	14%	
25000	Post	0%	0%	0%	0%	0%	4
	Pre	25%	25%	25%	25%	0%	
50000	Post	0%	0%	0%	0%	0%	4
	Pre	25%	25%	25%	25%	0%	
75000	Post	0%	0%	0%	0%	0%	3
	Pre	0%	0%	0%	0%	0%	
100000	Post	0%	0%	0%	0%	0%	2
	Pre	0%	0%	0%	0%	0%	

4. Discussion

Correlations between earthquakes and volcanic eruptions (VEI >2) have been shown in earlier studies (Linde and Sacks 1998; Manga and Brodsky 2006), suggesting that earthquakes can trigger volcanic eruptions, even at teleseismic distances. These studies showed that eruptions were most likely to occur within a day or two of large earthquakes. When we used a similar analysis to compare PDS estimates with more subtle SO_2 emission measurements we found no notable association. It was not possible to determine a standard for the length of time in which most SO_2 responses occurred following an earthquake, nor was it possible to determine a consistent level of PDS needed to trigger an SO_2 response at any of the volcanoes in this study. While this delay time method has been successful at establishing the significance of earthquake-volcano interactions when full eruptions are considered, our SO_2 dataset may be too incomplete for this type of comparison. For example, after visually inspecting the full SO_2 time series plot for Ambrym-Gaua with the baseline indicated (figure A.2) it became apparent that many of the earthquakes occurred when SO_2 output was below the calculated baseline amount. This led to instances when both a pre- and post-earthquake window occurred when SO_2 output was low enough that it was not considered in the delay-time analysis.

Our delay-time analysis used a method to determine a baseline for SO_2 degassing that may be useful for other types of studies where long-term background emissions are needed. A reliable measure of background SO_2 can be calculated for any volcano, given the limitations of OMI. These, briefly, are the influence of atmospheric conditions on SO_2 retrieval, the altitude sensitivity of the measurements, and the degeneration of the sensor and subsequent row anomaly. As previously mentioned, these issues can be addressed in the course of an analysis of the SO_2 mass dataset. Additionally, this method may be used for analysis of shorter periods of time, to investigate how baseline SO_2 output may correspond with observed changes in over-all activity patterns.

The method of determining average SO_2 levels in windows before and after earthquakes was effective for distinguishing between volcanic systems that were likely to have been affected by earthquake-caused shaking. By considering each volcano separately the connection between earthquakes and subtle changes in activity can be more easily identified. It is apparent from the data that the volcanoes included in this study responded differently to the dynamic stress generated by earthquakes. Two distinct categories emerged in the course of this study: 'open-vent' volcanoes with continuous, persistent degassing, (e.g., through lava lakes), showed a clear connection of elevated SO_2 output following earthquakes that generate high PDS, while volcanoes undergoing cyclic activity that may include conduit plugging seemed to demonstrate reduced SO_2 following such earthquakes. In this study only Rabaul-Ulawun did not indicate a susceptibility to changes in stress due to earthquakes manifested by degassing activity.

Ambrym-Gaua, Erta Ale, Villarrica, and Turrialba all demonstrated an SO_2 response following an earthquake with an occurrence rate at least 10% higher than the expected rate of occurrence. Ambrym-Gaua, Erta Ale, and Turrialba responded to earthquakes that generated at least 5 kPa of PDS, and the connection was clear when the minimum ratio of post- to pre- earthquake SO_2 levels was only 1.2. In the case of Villarrica the connection was clear when the earthquake catalog was subset to include earthquakes that generated at least 25 kPa PDS. Ambrym, Gaua, Erta Ale, and Villarrica share the feature of an episodically active lava lake during the study period. This common feature suggests that the balance of the volcanic system that can maintain a lava lake is more easily disturbed by the perturbations of small dynamic stress changes, and that the system will respond very quickly by degassing SO_2 as it re-equilibrates. Persistent lava lakes are maintained by the convection of magma, typically low-viscosity basalt, within the lake and feeder conduit driven by degassing (Stevenson and Blake 1998). According to Oppenheimer et al, (2009) the magma within the lake is essentially degassed, and emitted gas comes from new magma pulses from a deeper magma chamber. These deeper pulses of gas could be shaken as earthquake-generated dynamic stress passes through the volcanic system, causing the gas to escape rapidly. That rapid degassing would in turn be detected as an increase in SO_2 that continues until the system re-equilibrates. While Turrialba does not contain a lava lake, a dominant style of activity during the study period consisted of constant open vent degassing of SO_2. According to SI GVP reports, the level of SO_2 degassing forced the migration of local populations and was apparent in the destruction of vegetation near the vents. A constantly degassing system such as Turrialba would indicate a high degree of magmatic convection, even without the presence of a lava lake, and as such, be susceptible to the effects of dynamic stress.

A possible mechanism for increased degassing in response to passing seismic waves is rectified diffusion. Volatile solubility decreases during the expansion phase of the seismic wave, causing the volatiles to exsolve into the bubbles already present in the magma. The contraction phase of the wave causes the bubble to lose some of the volatiles, but less than what was gained during expansion because the surface are of the bubble is smaller when pressure is high. As the seismic waves pass the process is repeated, resulting in a pumping of volatiles into the bubbles (Ichihara and Brodsky 2006). While previous research (e.g. Manga and Brodsky 2006) has suggested that the increase of pressure due to rectified diffusion in a confined system is not likely to trigger an eruption, in the case of a very open system it could explain an increase in passively degassed SO_2. This process requires compressional waves and will not generally be valid for Love waves, but some conversion of SH to P is likely in magmatic systems.

Bagana, Merapi-Semeru, and Fuego-Pacaya did not demonstrate any correlation between earthquakes and subsequent elevated SO_2, at any level of PDS or SO_2 ratio. In all cases elevated SO_2 output occurs less frequently post-earthquake than expected from the full time

series analysis. However, the frequency of elevated SO_2 output is much higher than expected pre-earthquake. Merapi-Semeru and Fuego-Pacaya both demonstrate this inverse relationship at all levels of PDS and SO_2 ratio thresholds. Additionally, Bagana demonstrates this when earthquakes generating at least 5 kPa PDS are considered, and the SO_2 ratio is less than 1.6. These results indicate that these volcanoes are not susceptible to the effect of dynamic stress from tectonic earthquakes, regardless of the magnitude of PDS, at least with respect to their degassing activity. Merapi-Semeru and Bagana were in the process of dome-building during the time of this study. Bagana erupts high viscosity andesite lava, while Merapi and Semeru erupt basaltic-andesite lava. Dome-building is characterized by periods of lava extrusion alternating with low or no activity. Often there is a period of dome building followed by an explosive dome-collapse eruption, driven by a build-up of pressure after the vent is plugged by the viscous magma. This cyclic activity can be due to changes in gas pressure and surges of dome growth (Melnik and Sparks 2005). When the vent is plugged degassed SO_2 largely remains trapped in the magma chamber and conduit, causing an increase in pressure. Although neither Fuego nor Pacaya were undergoing long-term dome-building, the short term cyclic activity at Fuego during 2005-2007 suggests that the degassing was primarily controlled by the accumulation of gas (Lyons et al. 2009). Dynamic stress from earthquakes may influence the rate of pressure increase, by causing more rapid exsolution of gas. However, this is not measurable using the methods in this study. The pairing of Fuego and Pacaya because of proximity for SO_2 analysis introduces some complexity as the two volcanoes have different eruptive styles. Pacaya was an open, freely degassing system during this study period, and has shown an apparent direct relationship between seismic waves and SO_2 emission (Dalton 2009). The ambiguity in SO_2 response to dynamic stress for Fuego-Pacaya could be due to the manner in which the volcanoes were analyzed, or that any subtle change in degassing was below the detection sensitivity of the OMI SO_2 measurements.

5. Conclusion

This study investigated the connection between large, shallow tectonics earthquakes and temporally related variations in volcanic activity, as indicated by SO_2 output, at 13 global volcanoes. The results of the study indicate that the susceptibility of a volcanic system is in part dependent on magma composition and eruptive style. Very open systems, with lower viscosity magma, such as those with lava lakes, where passive degassing is constant, exhibit a high correlation between elevated SO_2 output and earthquake occurrence. Those systems with more dominant controls on degassing, such as during lava dome building, and higher viscosity magmas exhibit an inverse relationship, where SO_2 output was elevated before the earthquake occurred.

Future work for this study should include steps to further minimize error in the SO_2 time series, using complementary data such as wind speed and direction, as well as interpolation of values for pixels within the row anomaly. Additionally, a more specific investigation of SO_2 individual volcanoes, avoiding any pairing, could reduce error and provide greater insight. More work could be done to refine the seismogram modeling, with the goal of incorporating rupture directivity effects. We would also investigate narrower windows of pre- and post- earthquake SO_2 for the volcanoes that had a higher occurrence of elevated SO_2 pre-earthquake than was expected to further understand the relationship between degassing and dynamic stress in those regimes.

6. References

Carn SA, Krueger AJ, Arellano S, Krotkov NA, Yang K. 2008. Daily monitoring of Ecuadorian volcanic degassing from space. Journal of Volcanology and Geothermal Research 176(1):141-150.

Cigolini C, Laiolo M, Coppola D. 2007. Earthquake-volcano interactions detected from radon degassing at Stromboli (Italy). Earth and Planetary Science Letters 257(3-4):511-525.

Dalton M. 2009. Understanding volcanic processes at Pacaya volcano, Guatelmala using UV camera measurements of sulfur dioxide and coincident infrasound and seismicity [PhD Dissertation]. Houghton, MI. Michigan Technological University.

De la Cruz-Reyna S, Tárraga M, Ortiz R, Martínez-Bringas A. 2010. Tectonic earthquakes triggering volcanic seismicity and eruptions. Case studies at Tungurahua and Popocatépetl volcanoes. Journal of Volcanology and Geothermal Research 193(1-2):37-48.

Delle Donne D, Harris AJL, Ripepe M, Wright R. 2010. Earthquake-induced thermal anomalies at active volcanoes. Geology 38(9):771-774.

Eggert S, Walter TR. 2009. Volcanic activity before and after large tectonic earthquakes: Observations and statistical significance. Tectonophysics 471(1-2):14-26.

Fischer TP, Roggensack K, Kyle PR. 2002. Open and almost shut case for explosive eruptions: Vent processes determined by SO2 emission rates at Karymsky volcano, Kamchatka. Geology 30(12):1059-1062.

Harris AJL, Ripepe M. 2007. Regional earthquake as a trigger for enhanced volcanic activity: Evidence from MODIS thermal data. Geophysical Research Letters 34(2).

Herrmann RB. 2002. Computer programs in seismology v. 3.30.

Hill DP, Reasenberg PA, Michael A, Arabaz WJ, Beroza G, Brumbaugh D, Brune JN, Castro R, Davis S, dePolo D et al. . 1993. Seismicity Remotely Triggered by the Magnitude 7.3 Landers, California, Earthquake. Science 260(5114):1617-1623.

Hill DP, Pollitz F, Newhall C. 2002. Earthquake--Volcano Interactions. Physics Today 55(11):41-47.

Hill DP. 2008. Dynamic Stresses, Coulomb Failure, and Remote Triggering. Bulletin of the Seismological Society of America 98(1):66-92.

Ichihara M, Brodsky EE. 2006. A limit on the effect of rectified diffusion in volcanic systems. Geophysical Research Letters 33(2):L02316.

Linde AT, Sacks IS. 1998. Triggering of volcanic eruptions. Nature 395(6705):888-890.

Lyons JJ, Waite GP, Rose WI, Chigna G. 2009. Patterns in open vent, strombolian behavior at Fuego volcano, Guatemala, 2005–2007. Bulletin of Volcanology 72(1):1-15.

Manga M, Brodsky E. 2006. Seismic triggering of eruptions in the far field: Volcanoes and Geysers. Annual Review of Earth and Planetary Sciences 34(1):263-291.

Melnik O, Sparks RSJ. 2005. Controls on conduit magma flow dynamics during lava dome building eruptions. Journal of Geophysical Research 110(B2):B02209.

Oppenheimer C, Lomakina AS, Kyle PR, Kingsbury NG, Boichu M. 2009. Pulsatory magma supply to a phonolite lava lake. Earth and Planetary Science Letters 284(3-4):392-398.

Prejean SG, Hill DP, Brodsky EE, Hough SE, Johnston MJS, Malone SD, Oppenheimer DH, Pitt AM, Richards-Dinger KB. 2004. Remotely Triggered Seismicity on the United States West Coast following the Mw 7.9 Denali Fault Earthquake. Bulletin of the Seismological Society of America 94(6B):S348-359.

Shinohara H. 2008. Excess degassing from volcanoes and its role on eruptive and intrusive activity. Reviews of Geophysics 46(4):RG4005.

Stevenson DS, Blake S. 1998. Modelling the dynamics and thermodynamics of volcanic degassing. Bulletin of Volcanology 60(4):307-317.

Van Der Lee S. 1998. Observations and origin of Rayleigh-wave amplitude anomalies. Geophysical Journal International 135(2):691-699.

Velasco AA, Ammon CJ, Farrell J, Pankow K. 2004. Rupture Directivity of the 3 November 2002 Denali Fault Earthquake Determined from Surface Waves. Bulletin of the Seismological Society of America 94(6B):S293-299.

Walter TR, Amelung F. 2007. Volcanic eruptions following M ≥ 9 megathrust earthquakes: Implications for the Sumatra-Andaman volcanoes. Geology 35(6):539.

Walter TR, Wang R, Zimmer M, Grosser H, Lühr B, Ratdomopurbo A. 2007. Volcanic activity influenced by tectonic earthquakes: Static and dynamic stress triggering at Mt. Merapi. Geophysical Research Letters 34(5).

Walter TR, Wang R, Acocella V, Neri M, Grosser H, Zschau J. 2009. Simultaneous magma and gas eruptions at three volcanoes in southern Italy: An earthquake trigger? Geology 37(3):251-254.

Watt S, Pyle D, Mather T. 2009. The influence of great earthquakes on volcanic eruption rate along the Chilean subduction zone. Earth and Planetary Science Letters 277(3-4):399-407.

Wright R, Flynn LP, Garbeil H, Harris AJL, Pilger E. 2004. MODVOLC: near-real-time thermal monitoring of global volcanism. Journal of Volcanology and Geothermal Research 135(1-2):29-49.

Yang K, Krotkov NA, Krueger AJ, Carn SA, Bhartia PK, Levelt PF. 2007. Retrieval of large volcanic SO2 columns from the Aura Ozone Monitoring Instrument: Comparison and limitations. Journal of Geophysical Research 112(D24).

Yang K, Liu X, Krotkov NA, Krueger AJ, Carn SA. 2009. Estimating the altitude of volcanic sulfur dioxide plumes from space borne hyper-spectral UV measurements. Geophysical Research Letters 36(10):L10803.

Appendix A: data plots

Table A.1: Earthquake Catalog

YEAR	MONTH	DAY	TIME	LAT	LONG	DEPTH	(Mw)
2004	1	3	162321.02	-22.253	169.683	22	7.1
2004	2	5	210502.84	-3.615	135.538	16	7
2004	2	7	24235.21	-4.002	135.023	10	7.3
2004	9	5	100707.82	33.07	136.618	14	7.2
2004	9	5	145718.61	33.184	137.071	10	7.4
2004	10	9	212653.69	11.422	-86.665	35	7
2004	11	11	212641.15	-8.152	124.868	10	7.5
2004	11	15	90656.56	4.695	-77.508	15	7.2
2004	11	22	202623.9	-46.676	164.721	10	7.1
2004	11	26	22503.31	-3.609	135.404	10	7.1
2004	12	23	145904.41	-49.312	161.345	10	8.1
2004	12	26	5853.45	3.295	95.982	30	9.1
2005	3	28	160936.53	2.085	97.108	30	8.6
2005	6	15	25054.19	41.292	-125.953	16	7.2
2005	7	24	154206.21	7.92	92.19	16	7.2
2005	10	8	35040.8	34.539	73.588	26	7.6
2005	11	14	213851.42	38.107	144.896	11	7
2006	1	2	61049.76	-60.957	-21.606	13	7.4
2006	2	22	221907.8	-21.324	33.583	11	7
2006	4	20	232502.15	60.949	167.089	22	7.6
2006	5	3	152640.29	-20.19	-174.12	55	8.6
2006	7	17	81926.68	-9.284	107.419	20	7.7
2006	8	20	34148.04	-61.029	-34.371	13	7
2006	11	15	111413.57	46.592	153.266	10	8.3
2006	12	26	122621.14	21.799	120.547	10	7.1
2007	1	13	42321.16	46.243	154.524	10	8.1
2007	1	21	112745.06	1.065	126.282	22	7.5
2007	3	25	4001.61	-20.617	169.357	34	7.1
2007	4	1	203958.71	-8.466	157.043	24	8.1
2007	8	15	234057.89	-13.39	-76.6	39	8
2007	9	2	10518.15	-11.61	165.762	35	7.2
2007	9	12	111026.83	-4.438	101.367	34	8.5
2007	9	12	234903.72	-2.625	100.841	35	7.9
2007	9	13	33528.72	-2.13	99.627	22	7
2007	9	30	52334.07	-49.271	164.115	10	7.4
2007	12	19	93027.93	51.36	-179.509	34	7.2
2008	2	20	80830.52	2.768	95.964	26	7.4
2008	2	25	83633.03	-2.486	99.972	25	7.2
2008	3	20	223257.93	35.49	81.467	10	7.2
2008	4	9	124612.72	-20.071	168.892	33	7.3

2008	4	12	3012.6	-55.664	158.453	16	7.1
2008	5	12	62801.57	31.002	103.322	19	7.9
2008	6	30	61743.02	-58.227	-22.099	8	7
2008	7	19	23928.7	37.552	142.214	22	7
2008	11	16	170232.7	1.271	122.091	30	7.4
2009	1	3	194350.65	-0.414	132.885	17	7.7
2009	1	3	223340.29	-0.691	133.305	23	7.4
2009	2	11	173450.49	3.886	126.387	20	7.2
2009	2	18	215345.16	-27.424	-176.33	25	7
2009	3	19	181740.47	-23.043	-174.66	31	7.6
2009	5	28	82446.56	16.731	-86.217	19	7.3
2009	7	15	92229.03	-45.762	166.562	12	7.8
2009	8	10	195538.73	14.099	92.902	24	7.5
2009	9	29	174810.99	-15.489	-172.095	18	8.1
2009	10	7	221851.24	-12.517	166.382	35	7.8
2009	10	7	231348.16	-13.093	166.497	31	7.4
2010	1	3	223627.96	-8.799	157.346	25	7.1
2010	1	12	215310.06	18.443	-72.571	13	7
2010	2	26	203126.97	25.93	128.425	25	7
2010	2	27	63411.53	-36.122	-72.898	22	8.8
2010	4	4	224043.1	32.297	-115.278	4	7.2
2010	4	6	221501.58	2.383	97.048	31	7.8
2010	5	27	171446.57	-13.698	166.643	31	7.1
2010	6	12	192650.46	7.881	91.936	35	7.5
2010	6	16	31627.55	-2.174	136.543	18	7
2010	7	18	133459.36	-5.931	150.59	35	7.3
2010	8	10	52344.98	-17.541	168.069	25	7.3
2010	9	3	163547.77	-43.522	171.83	12	7
2010	9	29	171125.94	-4.963	133.76	26	7

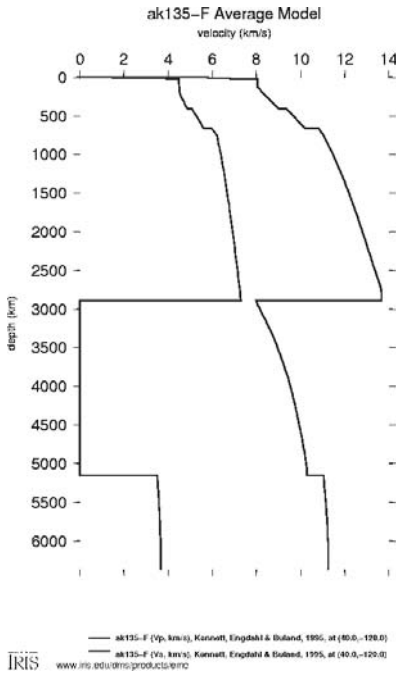

Figure A.1: AK135-F Earth Model, detailing the p- and s-wave velocity structure of the Earth.

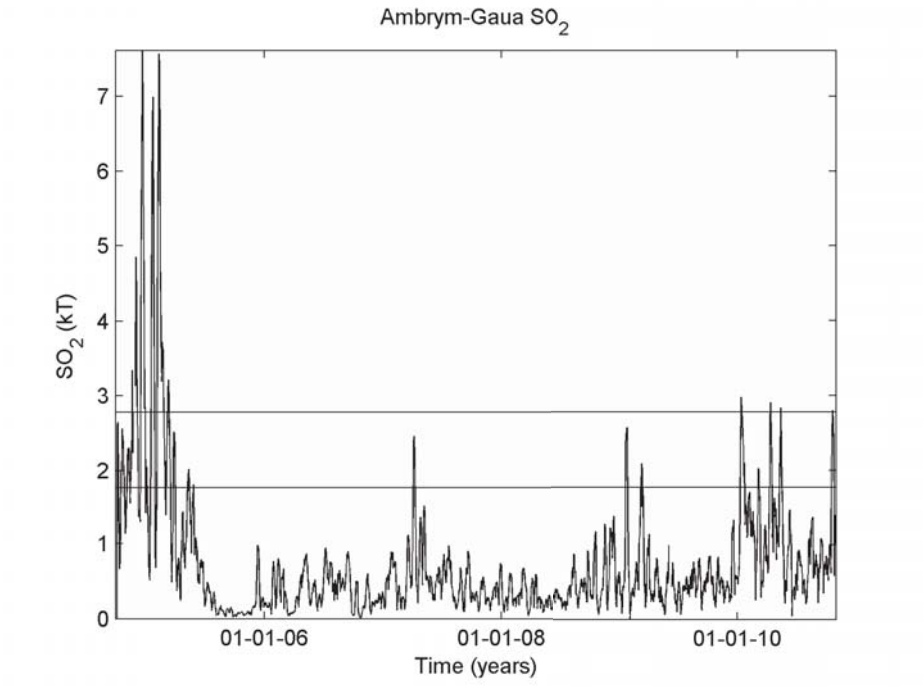

Figure A.2: Ambrym-Gaua SO_2 timeseries with baseline & baseline+2σ indicated.

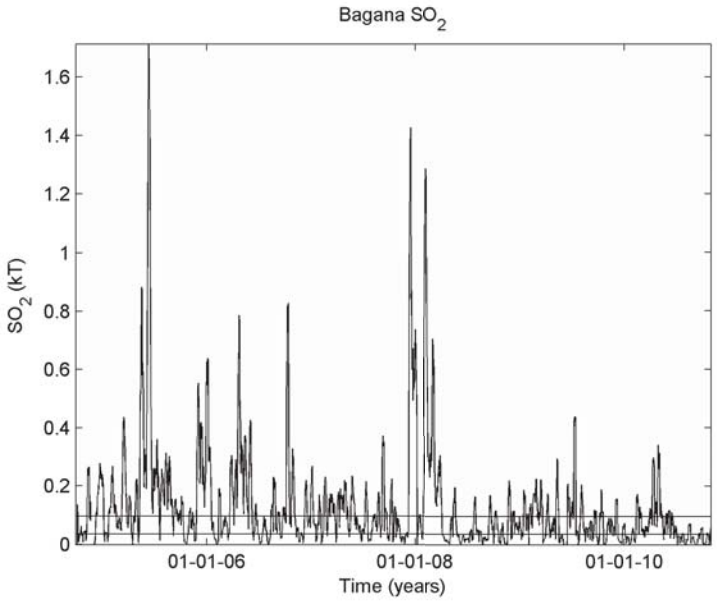

Figure A.3: Bagana SO_2 timeseries with baseline & baseline+2σ indicated.

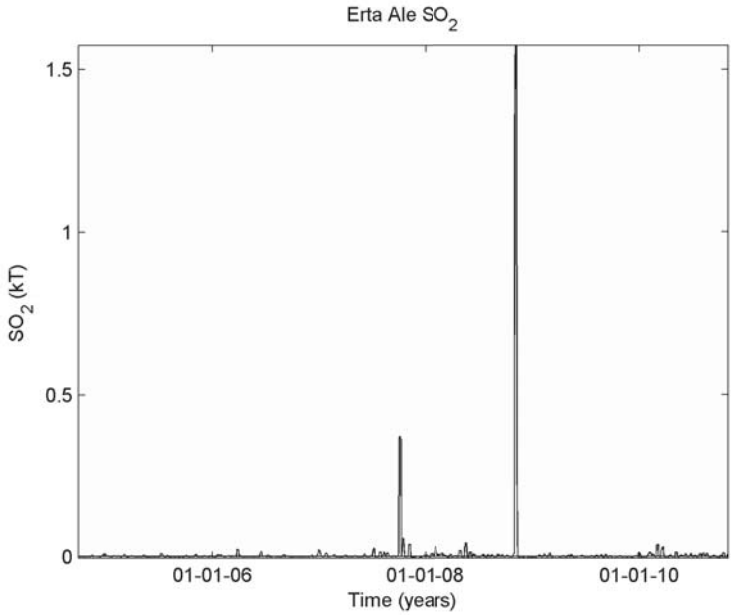

Figure A.4: Erta Ale SO_2 timeseries with baseline & baseline+2σ indicated

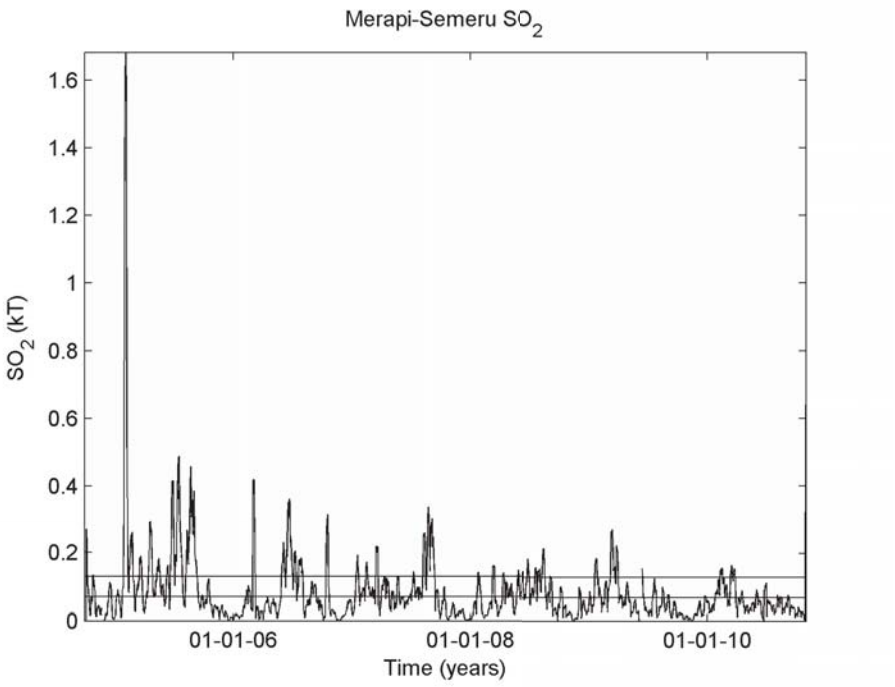

Figure A.5: Merapi-Semeru SO_2 timeseries with baseline & baseline+2σ indicated

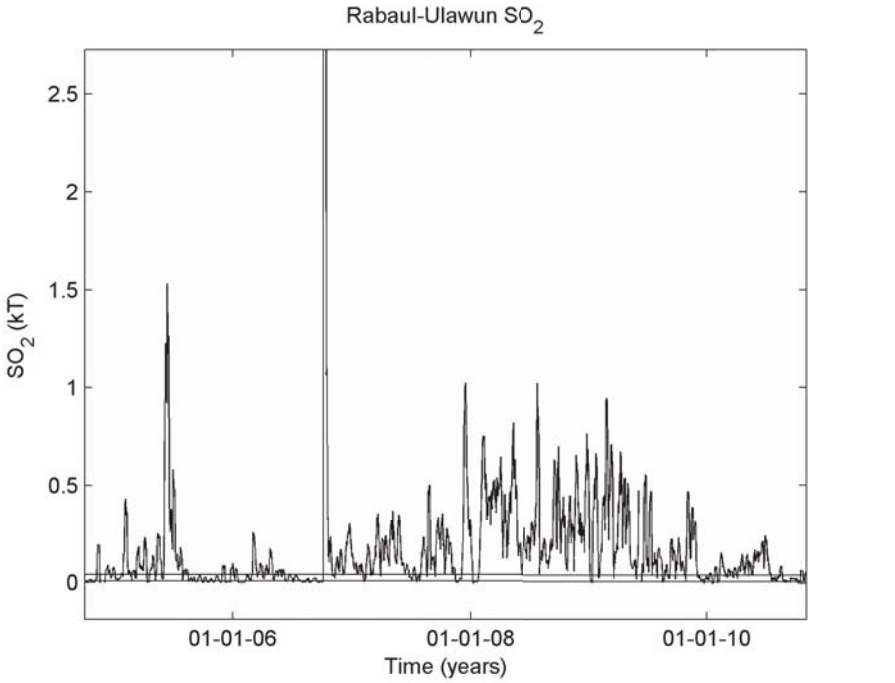

FigureA.6: Rabaul-Ulawun SO_2 timeseries with baseline & baseline+2σ indicated.

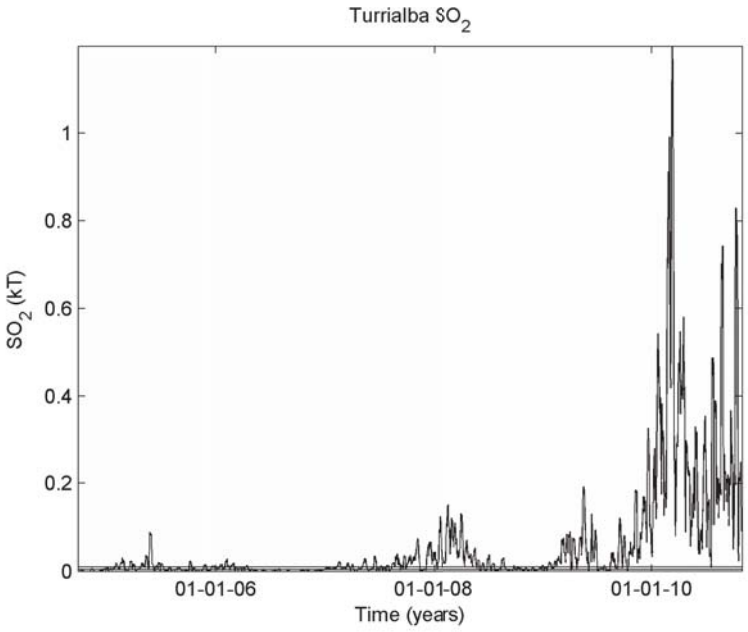

Figure A.7: Turrialba SO_2 timeseries with baseline & baseline+2σ indicated.